Application of a Supersonic Euler Code (SWINT) to Wing-Body-Tail Geometries

Jerry M. Allen* and James C. Townsend†
NASA Langley Research Center, Hampton, Virginia

Pressure and force calculations from the SWINT Euler code are presented and analyzed for a variety of configurations ranging from simple axisymmetric bodies to complex bodies with wings, tails, and inlets at speeds from low supersonic to low hypersonic Mach numbers. The SWINT results are compared with both experimental data and with results from simpler computational methods to assess the increased accuracy from the Euler solution. It is shown that SWINT gives excellent results on axisymmetric bodies for attached flow; however, a better method of simulating the separation process on such bodies is needed for increased leeside accuracy. Good leeside accuracy, however, is found on a 3 to 1 elliptical body. It is shown that SWINT gives realistic downstream interference effects, resulting in good predictions of the overall aerodynamics for complex wing-body-tail geometries. The QUICK-geometry system has been coupled with the SWINT code to provide a simplified geometry definition procedure for complex bodies. The QUICK method is shown to be a preferable alternative to the current method of inserting the body description directly into the code by FORTRAN statements.

Nomenclature

C_A = axial force coefficient, axial force/$q_\infty S$
C_ℓ = rolling moment coefficient, rolling moment/$q_\infty Sd$
C_m = pitching-moment coefficient, pitching moment/$q_\infty Sd$
C_N = normal force coefficient, normal force/$q_\infty S$
C_p = pressure coefficient, $P-P_\infty/q_\infty$
d = body diameter
L = body length
M = Mach number
P = static pressure
q = dynamic pressure
S = reference area
X = longitudinal distance from body nose
α = angle of attack
β = roll angle
ϕ_c = cone half-angle
ϕ = body circumferential angle

Subscripts

S = separation location
w = wing
∞ = freestream

Introduction

EXPERIMENTAL research over the past several years in wing-body-tail aerodynamics has demonstrated the desirability of incorporating nonaxisymmetric bodies into such configurations. This desirability results from both improved aerodynamics[1-3] and the need to meet physical size constraints.[4-6] Complementing this experimental research has been a development of new analytical tools with the potential for computing the aerodynamics of such configurations with more accuracy than traditional analysis methods. Much interest has been shown recently in a new computer code which seems ideally suited for this task—the Supersonic Wing Inlet Tail (SWINT) code. This code was developed by researchers at the Naval Surface Weapons Center[7,8] to solve the inviscid Euler equations for supersonic flow about arbitrary-shaped bodies, including inlets.

Before any computational code can be routinely used as an analytical tool, extensive evaluations should be made to assess its computational accuracy and ease of operation over a variety of geometries and flow conditions. The object of this paper is to present such an assessment of the SWINT code. SWINT pressure and force computations are presented for a variety of configurations ranging from simple axisymmetric bodies to arbitrary-shaped bodies with wings, tails, and inlets at speeds from low supersonic to low hypersonic Mach numbers. These computations are evaluated by comparing them with both experimental data and calculations from simpler classes of calculation techniques, including linear theory,[9,10] linear theory corrected for vortices (LRCDM2[11] and NOZVTX[12]), full-potential theory (NCOREL[13]), and hypersonic impact theory (HABP[14]).

Background

SWINT Code

The SWINT code computes solutions of the steady, three-dimensional Euler inviscid-flow equations in their weak conservation form. The equations are approximated as finite differences using the MacCormack second-order explicit predictor-corrector scheme. They are solved by space marching, utilizing the hyperbolic nature of the equations for supersonic flow. The bow shock is computed explicitly at each step using the Rankine-Hugoniot relations. Internal shocks are captured because of the conservative form of the flow variables.

The computational grid for each step is generated in physical space as the step is made. One set of grid lines is straight, radiating from a point within the body, and the other set is circumferential, fitted between the body and the bow shock. Although provision is made in SWINT for clustering the grid in each direction, clustering was not used to obtain the results presented here. All but one of the computations presented were made with a grid for only the right half of the configuration, assuming a vertical plane of symmetry. However, one configuration incorporated asymmetric fin deflections, so that a full 360 deg circumferential grid was needed for it. About 13 circumferential grid lines were found

Presented as Paper 85-1811 at the AIAA Atmospheric Flight Mechanics Conference, Snowmass, CO, Aug. 19-21, 1985; received Nov. 17, 1985; revision received Feb. 6, 1986.

*Aerospace Technologist, Fundamental Aerodynamics Branch, High-Speed Aerodynamics Division. Associate Fellow AIAA.

†Aerospace Technologist, Computational Methods Branch, High-Speed Aerodynamics Division. Member AIAA.

to be sufficient in all cases reported here. The number of radial lines ranged from 13 for simple shapes to 35 for configurations with rapid geometry changes in the circumferential direction.

In order to produce an efficient method, wing and tail fins are treated separately from the body flow computation using an approximation which considers the fins to be thin and to lie along radial lines of the grid system. This approximation assumes that the boundary conditions for the position, thickness, and deflection of any fin can be applied in the plane of the radial grid line on which it lies. Sharp-lipped inlets are treated by swallowing the flow at the inlet face and rezoning the grid to make the inlet cowl part of the body grid boundary.

For convenience, the more complex configurations were run in several stages of at most 900 steps each. The CPU execution times on a CDC Cyber 175 computer were as much as 9 min for the sum of these stages on one configuration. Computational difficulties encountered in regions of rapid geometry change were generally overcome by decreasing the step size in that region.

QUICK-Geometry Coupled With SWINT Code

One unusual aspect of the SWINT code is that it was written so that geometry descriptions are inserted directly into the code by FORTRAN statements. This process proves to be fairly straightforward for fins and simple axisymmetric bodies. For bodies of more complicated shapes, however, writing correct FORTRAN inputs can prove to be very difficult and time consuming.

Because there is no geometry package available for the SWINT code, researchers at the Langley Research Center have coupled the code with the QUICK-geometry system to make it more easy to use for general body shapes. This system was developed by the Grumman Aerospace Corporation under contract from Langley as a system for describing aircraft geometries in completely analytical form.[15,16] This geometry description was found to be ideally suited for the requirements of the SWINT code. The completely analytical nature of QUICK's geometry description has the advantages that cross-section definitions can be generated at any axial station, as is required by marching methods such as SWINT, and that first and second derivatives of the surface can be determined analytically at any point on the surface.

The geometry definition for the QUICK system is done entirely at a graphics computer terminal using interactive computer codes developed at Langley.[17,18] The left side of Fig. 1 shows the orginal discrete point definition for a typical cross section of the body shown in the upper right part of this figure. These points are used as a guide in defining a series of curve segments shown on the right side of Fig. 1, which analytically define this cross section. With all cross sections thus defined, the points determining these cross sections are connected by a series of body lines running generally from nose to tail. The configuration is now completely enveloped by a series of analytically defined curve segments. The SWINT code thus has access to the location, slope, and second derivative of any point on the body surface. The interactive method of generating input for the QUICK-geometry system saves considerable time over manual input and especially over the FORTRAN method of geometry definition. As an example, for the complicated, nonaxisymmetric body such as shown in Fig. 1, the QUICK-geometry definition was obtained in about one day, whereas the FORTRAN version required several weeks of an experienced programmer's effort.

Axisymmetric Bodies

For simple axisymmetric bodies, the FORTRAN method of geometry definition in the SWINT code is fairly simple and straightforward; hence, it is not necessary to use the QUICK-geometry system to define such bodies. In this section, SWINT calculations for these simple geometries are compared with both experimental data and with linear- and full-potential theories.

The full-potential code (NCOREL) contains large disturbance terms which are neglected in the linear-theory code (WOODWARD); whereas the Euler code (SWINT) adds the entropy terms which are neglected by the full-potential code. Therefore, comparing the calculated results from these three classes of theories will show the penalty incurred by neglecting the effects of these terms.

Cone

Figure 2 shows how the SWINT code predicts the pressure distributions on a 20 deg half-angle cone at Mach 2.5. Since the maximum angle of attack is about 21 deg, the leeside separation effects are negligible in these data. The SWINT results are compared with experimental data,[19] and with both linear and full-potential theories. The circumferential pressure distributions are plotted from the windward to the leeward meridian at the 96% body station; however, since the flow is conical the results are applicable to any longitudinal location.

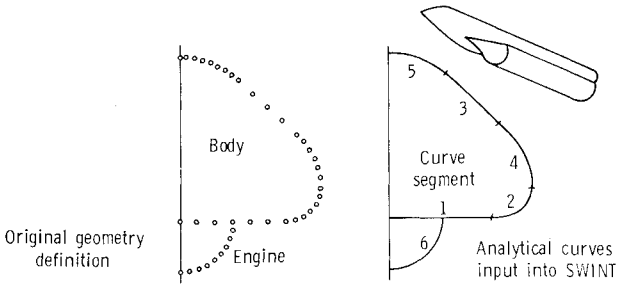

Fig. 1 QUICK-geometry technique.

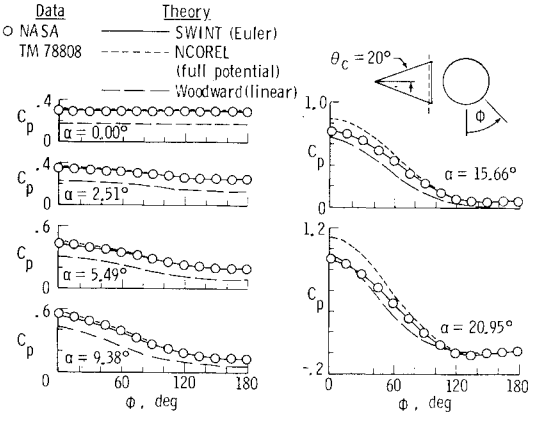

Fig. 2 Pressure distributions on cone at $M_\infty = 2.5$ and $X/L = 0.96$.

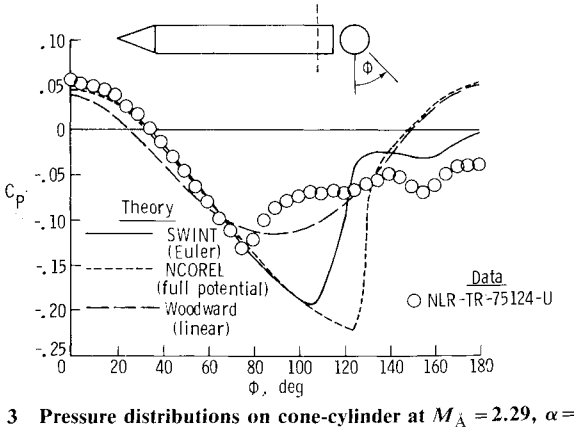

Fig. 3 Pressure distributions on cone-cylinder at $M_\infty = 2.29$, $\alpha = 12$ deg, and $X/L = 0.94$.

Even at the low angles of attack the linear-theory code is very inaccurate due to the large cone angle. The best agreement between the data and linear theory occurs at the highest angle of attack and appears to be entirely fortuitous. The full-potential code gives excellent results at the lower angles of attack ($\alpha \leq 9.38$ deg); however, at the higher angles of attack the theory begins to overpredict the data on the windward surface. The leeside pressures continue to be well predicted by the NCOREL code even at the higher angles of attack. The SWINT predictions are in excellent agreement with the data over the entire body at all angles of attack.

Two conclusions can be drawn from this figure. The first is that neglecting the large disturbance terms yields very inaccurate predictions for any conditions represented in this figure. The second is that neglecting the entropy terms yields inaccurate predictions where the shock wave is very strong, i.e., at the higher angles of attack on the windward surface.

Cone-Cylinder

These three codes are next used to predict the pressure distribution on a cone-cylinder at Mach 2.29 and 12 deg angle of attack, as shown in Fig. 3. The pressure data are taken from Ref. 20, which also presents flow visualization data showing that separation occurs on the leeside of the cylinder for these conditions. The pressure data were obtained at 7.5 body diam downstream of the nose and show from the discontinuity in the slope of the pressure distribution that separation occurs at about $\phi = 75$ deg at this body station.

The linear theory code is not very accurate even on the windward surface. This trend is consistent with the cone results discussed in Fig. 2. Also consistent is the fact that both NCOREL and SWINT are very accurate on the windward surface; however, after separation occurs both codes fail to predict the experimental pressures. Since neither code contains the viscous terms that would be necessary for the prediction of boundary-layer separation effects, both predict that the crossflow velocities continue to expand around the body, resulting in decreasing pressures instead of the separation that actually occurred. Although still inaccurate, the SWINT results follow the trend of the data better than the NCOREL results on the leeside. Note that the NCOREL pressures on the leeside are somewhat compensating; e.g., the pressures are too low on the outboard leeside (90 deg $< \phi <$ 130 deg) and too high on the inboard leeside (130 deg $< \phi <$ 180 deg). The integration of these pressures would give NCOREL normal force estimates which could appear to be fairly accurate. This trend was also noted in Ref. 21 in examining NCOREL pressures on an elliptical body.

In an effort to simulate a more realistic leeside flowfield, the SWINT code was written with an optional separation-line model which the user may select to be included in the solution. Since no theoretical method of separation-line modeling exists for general bodies, an empirically derived model has been included in the SWINT code. This model is based entirely on axisymmetric-body data and calculates the location of the separation line as a function of angle of attack and longitudinal distance along the body. The manner in which the separation model affects the solution in SWINT can be explained with the aid of Fig. 4. The sketches on the left side of this figure represent a body on which leeside separation has occurred. If the separation option is selected, the crossflow velocities on the body surface near the separation line are rotated to be parallel to the line, as shown in the right part of the figure. The crossflow velocities near the line are thus greatly reduced, or even reversed, to simulate a separation point. It was found that the use of a separation-line model did not necessarily force the computed flow to separate at that line. Conversely, the flow sometimes separated without a specified separation line if enough vorticity was generated by shocks or artificial viscosity. This process is described and its implications for the SWINT solution are discussed more completely in Ref. 22.

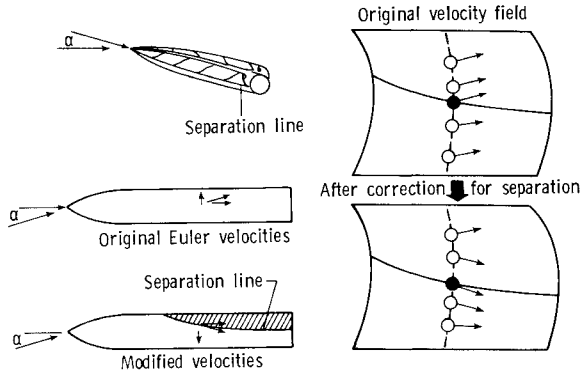

Fig. 4 SWINT separation-line model.

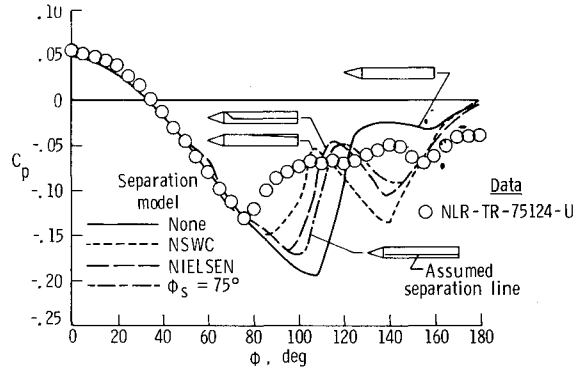

Fig. 5 Effect of separation-line model on SWINT pressure computation on cone-cylinder at $M_\infty = 2.29$, $\alpha = 12$ deg, and $X/L = 0.94$.

The user may either use the separation-line model included in the code, or can replace it with one of his own choosing. Figure 5 shows the effect of several models on the resulting SWINT calculated pressures on a replot of the Fig. 3 data. The curves represent pressure distributions with no separation-line model and three different models of the separation line. The "NSWC" model is the one included in the original SWINT code.[7,8] The "NIELSEN" model[23] was also developed from experimental data correlations, and is intended to provide a different separation line for cones and cylinders with a smooth transition between the two. Also, it is a function of Mach number. The "$\phi_s = 75$ deg" curve is a simple separation-line model located at 75 deg along the entire cylindrical part of the body, and it has been included in Fig. 5 to try to match the separation point at the data station. Note that the no-separation curve in Fig. 5 produces a rise in pressure on the leeside of the body (107 deg $< \phi <$ 125 deg) which resembles a pressure distribution produced by separation. This rise, however, is produced by a computed cross-flow shock near $\phi = 107$ deg, which results from rapid flow expansion around the body in the absence of separation.

For the Mach number and angle of attack in this figure, these three separation lines appear approximately as shown on the small sketches in the figure. Note that the specifying of separation has a strong effect on the calculated pressures, and the most conservative of the lines (NSWC) has the most effect. None of the models produce SWINT calculations which match the data in the separated region. Apparently, simply specifying a separation line is, in itself, not sufficient to properly model the separation process. Thus, if SWINT is to adequately predict separated-flow pressures, a better method of simulating viscous processes is needed.

Ogive-Cylinder With Cruciform Fins

In this section, the effects on the SWINT calculations of adding fins to an axisymmetric body are examined. The data are taken from Ref. 24 on a cruciform body-wing-tail con-

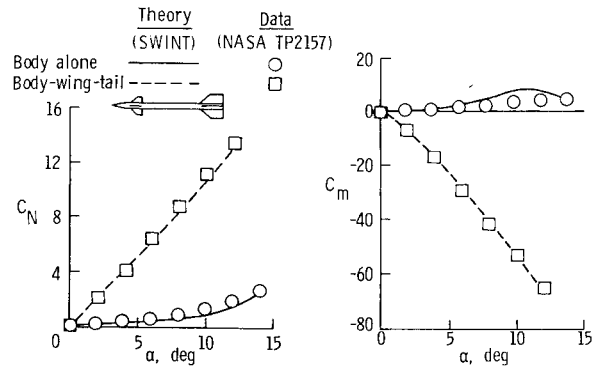

Fig. 6 Longitudinal characteristics on ogive-cylinder with cruciform fins at $M_\infty = 2.5$ and $\beta = 0$ deg.

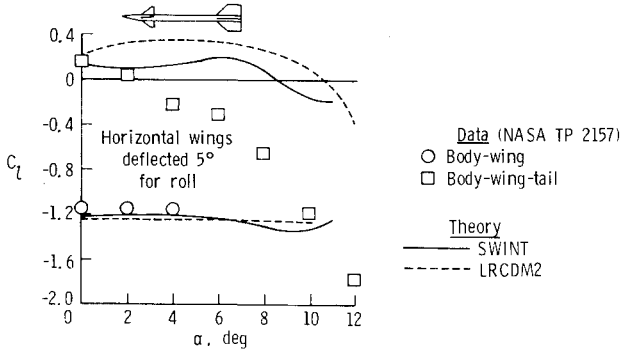

Fig. 7 Rolling moment characteristics on ogive-cylinder with cruciform fins at $M_\infty = 2.5$ and $\beta = 0$ deg.

figuration shown in the sketch in Fig. 6. The wings can be deflected for control purposes.

In this figure, the effects of angle of attack on the normal force and pitching moment coefficients for both body-alone and body-wing-tail combinations are shown. The fins are undeflected and the roll angle is zero. In the SWINT calculations, no separation-line specification was used for this configuration. For the body-alone comparisons, SWINT underpredicts the normal force because of the body separation problems noted in the cone-cylinder calculations; however, after the fins are added, SWINT is in very good agreement with the data. Since the fins completely dominate the body forces and moments on this configuration, the relatively weak calculated body loads are completely masked in the body-wing-tail calculations, yielding good overall results.

One interesting problem in configurations of this type is the lack of roll control capability at low angles of attack.[24] This problem is illustrated in Fig. 7, where rolling moment data are plotted as a function of angle of attack for both body-wing and body-wing-tail combinations. In both cases, the two horizontal wings are deflected 5 deg in opposite directions to produce a negative rolling moment. The vertical wings and all four tail fins are undeflected.

At low angles of attack, the data show that the deflected wings produce the proper rolling moment on the body-wing combination; however, the effect is completely cancelled when the tail fins are added. In fact, a small positive rolling moment is produced at zero angle of attack. This roll reversal occurs because the flowfield created by the deflected horizontal wings passes over the large tail fins, creating a rolling moment of about equal magnitude but opposite sign. This effect decreases with increasing angle of attack as the wing-induced flowfield begins to pass over the top of the tail fins.

These roll reversal data provide a good test of the ability of computational methods to calculate downstream interference effects, and it was used in Ref. 25 to investigate the ability of a

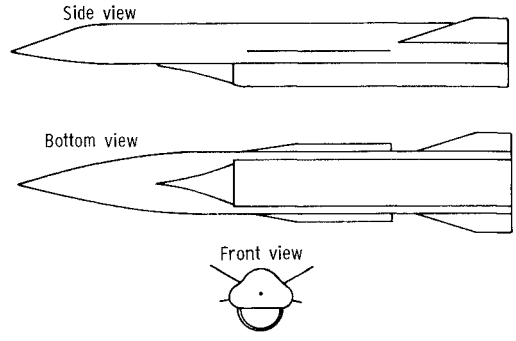

Fig. 8 Sketches of widebody concept.

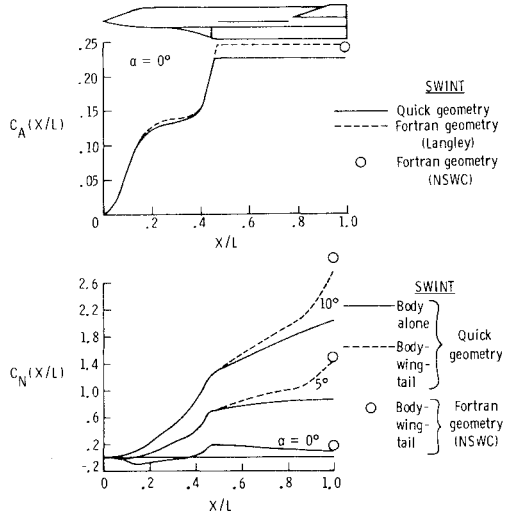

Fig. 9 Axial- and normal-force buildups on widebody concept at $M_\infty = 4.0$ and $\beta = 0$ deg.

preliminary version of LRCDM2 to calculate such flows. LRCDM2 calculations, which are essentially linear theory corrected for vortex effects, have been included in this figure along with the SWINT calculations.

Both SWINT and LRCDM2 give good results for the wing rolling moments and for the roll reversal effect on the complete configuration at the lower angles of attack. However, neither code properly accounts for the decrease in flowfield interference effects as angle of attack increases.

Nonaxisymmetric Bodies

In this section, SWINT results are presented and analyzed for three configurations with nonaxisymmetric bodies on which the QUICK-geometry technique was used to define the body geometries.

Widebody Concept

The first configuration is the widebody concept[6] sketched in Fig. 8. A cross section of the body was used in Fig. 1 in describing the QUICK-geometry technique. During the development of the SWINT code, the widebody geometry was supplied to NSWC researchers, who used it to check the code's performance for a nonaxisymmetric body. Thus FORTRAN geometry for this configuration was available and provided an opportunity for comparing SWINT results obtained by the FORTRAN and QUICK methods. Both FORTRAN and QUICK-geometry descriptions were used by SWINT for comparison at Mach 4 and angles of attack up to 10 deg.

The axial force buildup from SWINT on this configuration at zero angle of attack is shown at the top of Fig. 9. Both geometry techniques show sharp axial force increases on the nose and on the inlet spike and no increases downstream of the

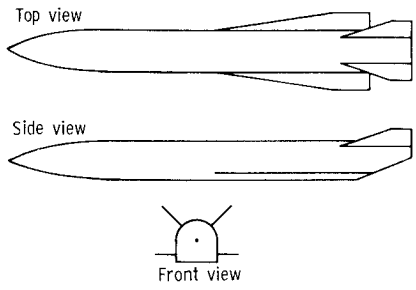

Fig. 10 Sketches of D-shaped body concept.

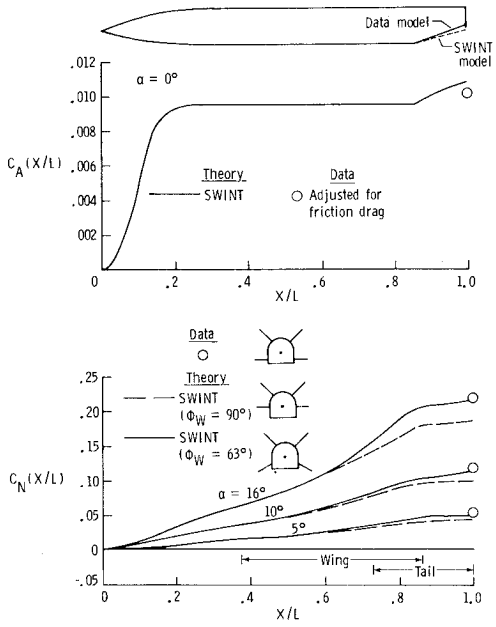

Fig. 11 Axial- and normal-force buildups on D-shaped body concept at $M_\infty = 6.0$ and $\beta = 0$ deg.

inlet. Note that there is no axial force increase due to the inlet itself. When the SWINT code detects an inlet from the discontinuous geometry definition, it captures the flow across the face of this discontinuity and produces no increment in forces. No axial forces were computed on the fins because they were modeled as zero-thickness surfaces.

Although both geometry descriptions give the same trend in axial force, there are small differences between the two. Examination of geometry plots from both techniques revealed that the QUICK geometry was smoother, thereby, resulting in a slightly lower axial force. Note that the FORTRAN geometry results obtained at NSWC and Langley are almost identical. Thus the differences between the FORTRAN and QUICK calculations result from real differences in geometry input into the SWINT code.

The normal force buildups on this configuration are shown on the bottom of Fig. 9 for angles of attack of 0, 5, and 10 deg. Both body-alone and body-wing-tail distributions are presented using the QUICK-geometry inputs, and overall body-wing-tail results are presented using the NSWC FORTRAN geometry calculations. No fin contributions to normal force is present at zero angle of attack, but their contribution is clearly evident as the angle of attack increases. As was noted in the axial force results, the FORTRAN geometry gives slightly higher normal forces than does the QUICK geometry at each angle of attack.

It should be emphasized, as mentioned earlier, that a large amount of time and effort was needed to define this body by FORTRAN statements as compared with the QUICK-geometry technique. Several weeks of programming resulting

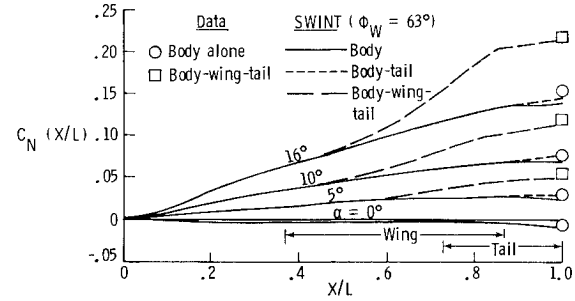

Fig. 12 Effect of fins on normal-force buildups on D-shaped body concept at $M_\infty = 6.0$ and $\beta = 0$ deg.

in about 470 lines of code were required to define this body and inlet by the FORTRAN technique. The QUICK-geometry definition was generated in a single day and resulted in a smoother geometry description. The QUICK-geometry definition has thus been shown to be a preferable alternative to the FORTRAN definition in describing complex geometries to the SWINT code. SWINT calculations for the remaining two configurations will thus be obtained exclusively from QUICK-geometry inputs.

D-Shaped Body Concept

The second configuration is the D-shaped body concept[4,5] sketched in Fig. 10. SWINT calculations are analyzed and compared with both experimental data and with the standard method of predicting hypersonic aerodynamics—the Hypersonic Arbitrary Body Program (HABP). The body has a flat undersurface and an inclined ramp near the aft end designed to accommodate an engine mounted underneath the body. The engine has not been included in either the data or calculations presented on this configuration. Two low aspect ratio wings are mounted low on the fuselage, and twin tails are mounted high on the afterbody. Both the wings and tails present computational challenges to the SWINT code.

One of the requirements of the thin-fin assumption of SWINT code is that fins must lie along radial lines from the computational axis; i.e., from the center of the body. The wings on this configuration do not fit this requirement, as can be seen from the model sketches; therefore, adjustments were made in the wing location described to SWINT.

The tail fins lie along radial lines, so they present no grid problems for SWINT; however, they are located in the leeside flow at high angles of attack. The shielding of these fins by the body is a well-known, serious deficiency of the isolated-panel HABP code.

The top of Fig. 11 shows the axial force buildup predicted by the SWINT code at zero angle of attack at Mach. 6.0 on the D-shaped body. A small modification of the ramp geometry near the aft end of the body was necessary, so that the computational axis in this region would lie within the body. Most of the axial force is produced on the nose of the body; however, a noticeable increase occurs on the ramp. Included for comparison is the measured axial force on this body adjusted by subtracting a computed laminar skin friction. The experimental and computed axial forces agree within a few percent.

The bottom of Fig. 11 shows the predicted normal force buildups on this configuration at angles of attack of 5, 10, and 16 deg at Mach 6.0. Because of the radial-fin restriction mentioned earlier, two sets of SWINT calculation were performed. In one set, the wings remained horizontal, but were raised to a higher position on the body so that they lie along the $\phi = 90$ deg grid line. This set of calculations is labeled "$\phi_w = 90$ deg" in the figure. In the second set, the vertical location of the original configuration's wing root chord was maintained, but the wings were rotated downward so that they extended along the $\phi = 63$ deg grid line. This set of calculations is labeled

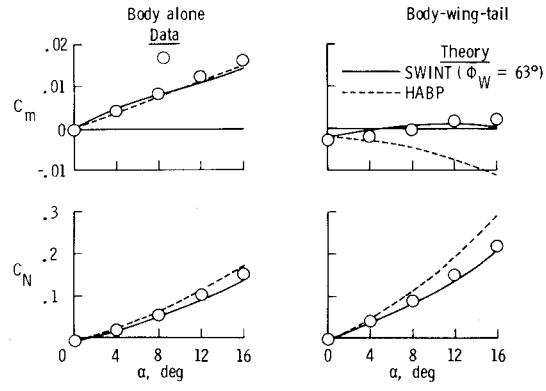

Fig. 13 Longitudinal characteristics on D-shaped body concept at $M_\infty = 6.0$ and $\beta = 0$ deg.

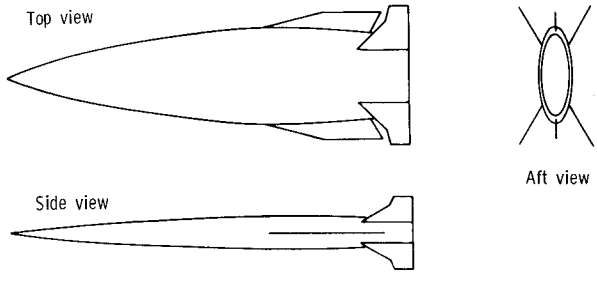

Fig. 14 Sketches of elliptical concept.

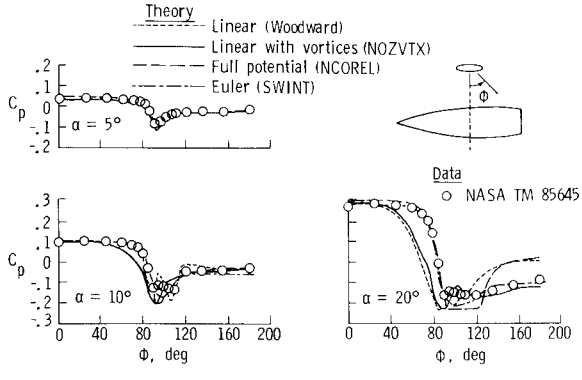

Fig. 15 Pressure distributions on elliptical concept at $M_\infty = 2.5$, $\beta = 0$ deg, and $X/L = 0.6$.

"$\phi_w = 63$ deg." Sketches of the experimental configuration and both sets of computational configurations are included. The $\phi_w = 63$ deg calculations are in very good agreement with the data; whereas, the $\phi_w = 90$ deg calculations are somewhat low at each angle of attack. Hence, it appears that maintaining the correct vertical location of the wings was more important for computational accuracy than maintaining the correct angular orientation.

The effects of the shielded tail fins are shown in Fig. 12, where the normal force buildups for the $\phi_w = 63$ deg computational configuration are shown for body-alone, body-tail, and body-wing-tail combinations. Note that the SWINT code predicts a very strong effect from the wings, but very little effect from the tails. Also included in this figure are experimental data on this configuration for body-alone and body-wing-tail combinations. The data are in general slightly higher than the SWINT calculations, but the overall agreement is quite good.

In contrast to SWINT, however, the traditional code for predicting the aerodynamics of such configurations, the HABP code, overpredicts the effectiveness of these tail fins, as can be seen in Fig. 13. In this figure, pitching moment and normal force coefficients are shown as a function of angle of attack for the body-alone and body-wing-tail combinations at Mach 6.0. Shown for comparison with the experimental data are the predictions from SWINT and from HABP. For the body alone, both codes do an adequate job of predicting the data; however, for the body-wing-tail combination HABP overpredicts the normal force, primarily due to overestimating the effects of the tail fins. This difference is even more evident in the pitching moment results. Both data and SWINT predict a slightly unstable trend whereas HABP predicts that the configuration is stable, again due to overestimating the effectiveness of the tail fins. Hence, the shielding effect in the leeside flow of this hypersonic configuration, which has been known to be a problem for the HABP code, is well predicted by SWINT.

Elliptical Concept

The last configuration is the 3 to 1 elliptical concept[1] sketched in Fig. 14. Because of the wealth of data that exists on this configuration, it has been used for several years as a test bed to evaluate developing computational methods. Force and moment,[2] pressure,[26] and vapor screen[21] data have been used in Refs. 21 and 27 to analyze several computational methods. In this section, SWINT predictions will be added to this analysis.

Figure 15 shows circumferential pressure distributions on this body at the 60% body station at angles of attack of 5, 10, and 20 deg at Mach 2.5. Shown for comparison are predictions from four computational methods representing different classes of solution. This figure is essentially a reproduction of Fig. 9 from Ref. 21 with the SWINT solution added. Only the SWINT results will be analyzed in this paper. Interested readers are referred to Ref. 21 for a detailed analysis of the other prediction methods on this body.

Even at the highest angle of attack, the SWINT predictions are accurate on both the windward and leeward surfaces. It is known from vapor-screen photographs on this body[21] that strong vortices develop on the leeside, and yet SWINT closely estimates the leeside pressures. This result is opposite to those presented in Fig. 3 on the cone-cylinder body, where it was shown that SWINT did not accurately predict the leeside pressures on that body after separation occurred.

Examination of the calculated crossflow velocities on these two bodies revealed that the large expansion around the leading edge of the elliptical body produced a more realistic circulating flowfield than was produced in the cone-cylinder calculations. The vortical flowfield was thus more correctly modeled on the elliptical body, which produced better agreement with the pressure data. The leeside pressure agreement is, in fact, comparable to that from the NOZVTX code, which directly models leeside vortices, and is much better than the linear theory and full-potential theory codes. It should be emphasized that this SWINT result was obtained without specifying any separation line on this body.

The top of Fig. 16 shows the axial force buildup predicted by SWINT for this body at zero angle of attack. Since the area distribution of this body is the same as an Adams minimum drag body,[28] the axial force distribution is very smooth compared to the previous bodies analyzed. The relative drag contributions of the nose and boattail sections can be easily seen in this type of plot. Shown for comparison is the experimental axial force from Ref. 2 in which the calculated turbulent skin friction drag has been subtracted. Excellent agreement is seen between SWINT and experiment.

The normal force buildups are shown at the bottom of Fig. 16 for both the body-alone and the complete configuration. Note that the bulk of the normal force on this configuration comes from the body instead of the fins. This is in contrast to the results on the axisymmetric, cruciform configuration shown in Fig. 6 in which most of the normal force came from the fins. Shown for comparison are the experimental normal

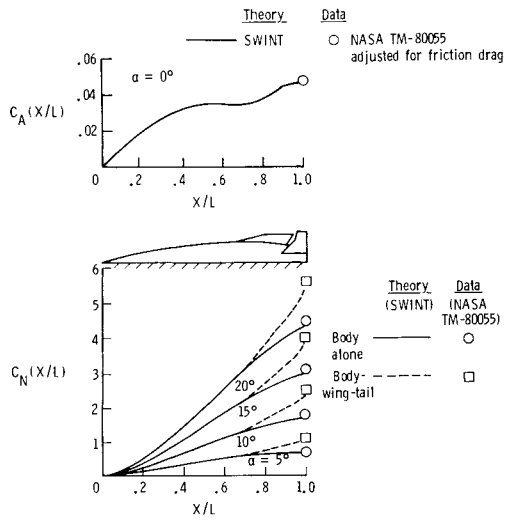

Fig. 16 Axial- and normal-force buildups on elliptical concept at $M_\infty = 2.5$ and $\beta = 0$ deg.

force values.[2] The experimental data are always slightly higher than the SWINT calculations, but the increments due to fins are well predicted. This trend is in agreement with that on the D-shaped configuration discussed previously.

The good predictions shown in this figure by the SWINT code is very close to that shown in Ref. 21 by the NCOREL code. However, analysis in Ref. 21 of the pressure distributions revealed that the good NCOREL agreement was somewhat fortuitous due to compensating errors in the pressure predictions on the leeside of this body. The good agreement from the SWINT code shown in this figure is the result of well-predicted pressures on both sides of the body, as can be seen from Fig. 15.

Concluding Remarks

Pressure and force calculations from the SWINT Euler code have been presented and analyzed for a variety of configurations ranging from simple axisymmetric bodies to complex bodies with wings, tails, and inlets at speeds from low supersonic to low hypersonic Mach number. The SWINT results have been compared with both experiments data and with results from simpler computational methods to assess the increased accuracy from the Euler solution.

It was found that SWINT gave excellent results on axisymmetric bodies for attached flow; however, a better method of simulating the separation process on such bodies is needed for increased leeside accuracy. Good leeside results, however, were found for a 3 to 1 elliptical body. It was found that SWINT gave realistic downstream interference effects, resulting in good predictions of the overall aerodynamics for complex body-wing-tail geometries.

The QUICK-geometry system has been coupled with the SWINT code to provide a simplified geometry definition procedure for complex bodies. The QUICK method was shown to be a preferable alternative to the current method of inserting the body description directly into the code by FORTRAN statements.

References

[1]Graves, E. B., "Aerodynamic Characteristics of a Monoplanar Missile Concept With Bodies of Circular and Elliptical Cross Sections," NASA TM-74079, 1977.

[2]Graves, E. B. and Fournier, R. H., "Effect of Nose Bluntness and Afterbody Shape on Aerodynamic Characteristics of a Monoplanar Missile Concept With Bodies of Circular and Elliptical Cross Sections at a Mach Number of 2.50," NASA TM-80055, 1979.

[3]Graves, E. B. and Robins, A. W., "Supersonic Aerodynamic Trade Data for a Low-Profile Monoplanar Missile Concept," *Journal of Aircraft,* Vol. 17, Feb. 1980, pp. 95-98.

[4]Hunt, J. L. et al, "Hypersonic Airbreathing Missile Concepts Under Study at Langley," AIAA Paper 82-0316, 1982.

[5]Dillon, J. L., Marcum, D. C., Jr., Johnston, P. J., and Hunt, J. L., "Aerodynamic and Inlet Flow Characteristics of Several Hypersonic Airbreathing Missile Concepts," *Journal of Aircraft,* Vol. 18, April 1981, pp. 231-237.

[6]Hunt, J. L., Johnston, P. J., and Riebe, G. D., "Flow Fields and Aerodynamic Characteristics for Hypersonic Missiles with Mid-Fuselage Inlets," AIAA Paper 83-0542, 1983.

[7]Wardlaw, A. B. Jr., Baltakis, F. P., Soloman, J. L., and Hackerman, L. B., "An Inviscid Computational Method for Tactical Missile Configurations," NSWC TR 81-457, 1981.

[8]Wardlaw, A. B. Jr., Hackerman, L. B., and Baltakis, F. P., "An Inviscid Computational Method for Supersonic Missile Type Bodies—Program Description and User's Guide," NSWC TR 81-459, 1981.

[9]Woodward, F. A., "An Improved Method for the Aerodynamic Analysis of Wing-Body-Tail Configurations in Subsonic and Supersonic Flow. Part I-Theory and Application," NASA CR-2228, Part I, 1973.

[10]Woodward, F. A., "An Improved Method for the Aerodynamic Analysis of Wing-Body-Tail Configurations in Subsonic and Supersonic Flow. Part II-Computer Program Description," NASA CR-2228, Part II, 1973.

[11]Dillenius, M. F. E., "Program LRCDM2, Improved Aerodynamic Prediction Program for Supersonic Canard-Tail Missiles With Axisymmetric Bodies," NASA CR-3883, 1985.

[12]Mendenhall, M. R. and Perkins, S. C. Jr., "Prediction of Vortex Shedding From Circular and Noncircular Bodies in Supersonic Flow," NASA CR-3754, 1984.

[13]Siclari, M. J., "The NCOREL Computer Program for 3D Nonlinear Supersonic Potential Flow Computations," NASA CR-3694, 1983.

[14]Gentry, A. E., Smyth, D. N., and Oliver, W. R., "The Mark IV Supersonic-Hypersonic Arbitrary-Body Program Formulation—Volume III, Program Listing," AFFDL TR-73-159, Nov. 1973.

[15]Vachris, A. F. Jr. and Yaeger, L. S., "QUICK-GEOMETRY—A Rapid Response Method for Mathematically Modeling Configuration Geometry. Application of Computer Graphics in Engineering," NASA SP-390, 1975.

[16]Marconi, F. and Yaeger, L., "Development of a Computer Code for Calculating the Steady Super/Hypersonic Inviscid Flow Around Real Configurations. Volume II-Code Description," NASA CR-2676, 1976.

[17]Adams, M. S., "Interactive Input for the QUICK-Geometry System—User's Manual," NASA TM-81933, 1981.

[18]Townsend, J. C., "Use of Interactive Graphics to Analyze QUICK-Geometry," NASA TM-83234, 1981.

[19]Townsend, J. C., Collins, I. C., Howell, D. T., and Hayes, C., "Surface Pressure Data on a Series of Conical Forebodies at Mach Numbers From 1.70 to 4.50 and Combined Angles of Attack and Sideslip," NASA TM-78808, 1979.

[20]Boersen, S. J., "Reynolds Number Effects on Pressure and Normal Force Distributions Along Conically Pointed Circular Cylinder at Free-Stream Mach Number of 2.3," NLR-TR-75124-U, 1975.

[21]Allen, J. M. and Pittman, J. L., "Analysis of Surface Pressure Distributions on Two Elliptical Missile Bodies," *Journal of Spacecraft and Rockets,* Vol. 21, Nov.-Dec. 1984, pp. 528-533.

[22]Adiason, M. I. and Krieger, R. J., "Evaluation of Vortex Wake Predictions in the SWINT Code," AIAA Paper 85-0450, 1985.

[23]Kuhn, G. D., private communications, Nielsen Engineering and Research, Inc., Mountain View, California.

[24]Blair, A. B. Jr., Allen, J. M., and Hernandez, G., "Effect of Tail-Fin Span on Stability and Control Characterisics of a Canard-Controlled Missile at Supersonic Mach Numbers," NASA TP-2157, 1983.

[25]Allen, J. M. and Blair, A. B. Jr., "Comparison of Analytical and Experimental Supersonic Aerodynamic Characteristics of a Forward Control Missile," *Journal of Spacecraft and Rockets,* Vol. 19, March-April 1982, pp. 155-159.

[26]Allen, J. M., Hernandez, G., and Lamb, M., "Body-Surface Pressure Data on Two Monoplane-Wing Missile Configurations With Elliptical Cross Sections at Mach 2.50," NASA TM-85645, 1983.

[27]Pittman, J. L. and Siclairi, M. J., "Nonlinear Aerodynamic Effects on Bodies in Supersonic Flow," *Journal of Aircraft,* Vol. 21, Oct. 1984, pp. 809-815.

[28]Adams, M. D., "Determination of Shapes of Boattail Bodies of Revolution for Minimum Wave Drag," NACA TN-3054, 1953.